



THE UNIVERSITY *of* EDINBURGH

Edinburgh Research Explorer

Coupled hybrid modelling within the Fire Dynamics Simulator; transient transport and mass storage

Citation for published version:

Ralph, B, Carvel, R & Floyd, J 2019, 'Coupled hybrid modelling within the Fire Dynamics Simulator; transient transport and mass storage', *Journal of Building Performance Simulation*.
<https://doi.org/10.1080/19401493.2019.1608304>

Digital Object Identifier (DOI):

[10.1080/19401493.2019.1608304](https://doi.org/10.1080/19401493.2019.1608304)

Link:

[Link to publication record in Edinburgh Research Explorer](#)

Document Version:

Peer reviewed version

Published In:

Journal of Building Performance Simulation

General rights

Copyright for the publications made accessible via the Edinburgh Research Explorer is retained by the author(s) and / or other copyright owners and it is a condition of accessing these publications that users recognise and abide by the legal requirements associated with these rights.

Take down policy

The University of Edinburgh has made every reasonable effort to ensure that Edinburgh Research Explorer content complies with UK legislation. If you believe that the public display of this file breaches copyright please contact openaccess@ed.ac.uk providing details, and we will remove access to the work immediately and investigate your claim.



Coupled hybrid modelling within the Fire Dynamics Simulator; transient transport and mass storage

Benjamin Ralph ^{*1}, Ricky Carvel¹, and Jason Floyd²

¹School of Engineering, The University of Edinburgh, The King's Buildings, Mayfield Road, Edinburgh EH9 3FG, Scotland, United Kingdom

²Jensen Hughes, 111 Rockville Pike, Suite 550, Rockville, MD 20850, USA

Abstract

Non-prescriptive design within fire engineering is becoming more prevalent as buildings get taller and more complex. This necessitates the increased use of reliable deterministic predictions; typically computational fluid dynamics-based models. Driven by time constraints, modellers are required to limit the domain to reduce wall time. This ignores the two-way coupling of a fire and a total building system. A neglect which could embody risk to life. One way to address this risk is the use of coupled hybrid modelling to expand the domain; explicitly quantifying risk-related quantities in the far field whilst maintaining practicable wall times. Fire Dynamics Simulator (FDS) version 5.5 opened the door to coupled hybrid modelling within FDS and introduced the HVAC network submodel. Until FDS version 6.5.3 the submodel did not account for transient transport or mass storage. In this work a new transient transport and mass storage subroutine has been introduced into HVAC which is available in FDS version 6.5.3 onwards. The relevant conservation equations and numerical solution are described. Successful verification cases are presented for various arrangements to test the implementation of the solution scheme. To demonstrate the benefits of the new method, a fire engineering test case is presented. The test case illustrates the potential risks contained within the pre-existing coupled hybrid modelling method. These risks include unrealistic predictions of hot layer height and head height temperatures and visibility. The test case demonstrates that the new coupled hybrid modelling method address these shortcomings and could form part of a most robust fire safety engineering solution. Based on experimental benchmarking exercises, recommended model bias factors are put forward. The new model implementation can be used by designers to quantitatively examine the fire hazard embodied within the two-way coupling of a fire and a total building system.

Keywords— coupled hybrid modelling; fire modelling; computational fluid dynamics; multiscale modelling; risk assessment; fire safety

Nomenclature

Greek Symbols

ϕ Conserved variable

ρ Gas density

kg/m³

*Corresponding author: b.ralph@ed.ac.uk

Roman Symbols

\bar{p}	Background pressure	Pa
A	Cross sectional area	m^2
c_p	Specific heat capacity	$\text{kJ}/(\text{kg K})$
D_α	Diffusion coefficient	m^2/s
F	Fan set	
g	Acceleration due to gravity	m/s^2
h	Specific enthalpy	kJ/kg
K	Loss coefficient	
L	Length	m
m	Mass	kg
p	Pressure	Pa
p_L	Pressure loss	Pa
q	Volume flow rate	m^3/s
R	Universal gas constant	$\text{kJ}/(\text{K mol})$
T	Temperature	K
t	Time	s
u	Gas velocity	m/s
V	Volume	m^3
W	Molecular weight	kg/mol
x	First dimension of space	m
Y	Species concentration	
z	Elevation	m

Superscripts

"	Flow rate per unit area (flux)
k	Iteration index
n	Time step index

Subscripts

α	Species index
∞	Ambient value
c	Duct cell index
f	Fan index
g	Gas field cell index
i	Upstream duct node index
j	Duct index

k	Downstream duct node index
V	Vent index
V	Vent-adjacent cell set (where used on a domain)
w	Wall cell index

Other Symbols

$-$	Cell centred value
δn	Normal unit vector
\cdot	First derivative of time
\sim	Extrapolated value or cell face value

1 Introduction

Performance-based or non-prescriptive design in fire safety is becoming more prevalent [1]. As part of these designs, fire engineers often use computational fluid dynamics (CFD)-based fire modelling tools (also called field models) to predict how fire and smoke may spread through a building [2]. Use of complex fire models is becoming commonplace as buildings get taller [3] and more complex [4].

Considering the total building system when carrying out these fire safety assessments is imperative [5]. Over half of fire fatalities in the UK, US, and Australia occur outside of the room of fire origin [6, 7, 8]. Over 65% of fire fatalities in the UK are caused by smoke inhalation [9]. The total building system, including shafts, ventilation systems and voids, strongly affects how a fire grows and how fire and smoke spreads through a building [10].

However, the construction industry is driven by time constraints [11]. Fire engineers and modellers are motivated to reduce the time required for analysis to take place [12]. This is often achieved by reducing the size of the domain of the field model calculation [13]. For example, it is impracticable to include every element of a complicated ventilation system within the field model domain.

Within this curtailed domain paradigm, the simulation generally does not account for the two-way coupling between the fire and the total building system. This ignores fire and smoke spread to the rest of the building and neglects how the building may affect how a fire grows and spreads. For example, within the current modelling paradigm, the potential for smoke from a fire at level 3 of a multistory hospital building spreading to an intensive care unit (ICU) at level 5 via the stairs or ventilation system is ignored as these elements are outside of the field domain. The designer and stakeholders would have no data to inform them that the ICU occupants could be at risk.

One solution to this is the use of coupled hybrid modelling. This modelling method comprises coupling a computationally cheap submodel to the more expensive field model to extend the domain of the calculation. This enables the modeller to explicitly output quantitative measures for far field parts of the building and examine the affect of the two-way coupling of the fire and the building.

Fire Dynamics Simulator (FDS) version 5.5 introduced a 1D network submodel which could be coupled to the field domain at vents. Prior to FDS version 6.5.3 this 1D network submodel (called ‘‘HVAC’’) instantaneously moved energy and matter from the inlet vent to the outlet vent within the field domain. There was no unsteady motion of mass or energy through the HVAC network subdomain. This meant that for calculations where time-dependent phenomena were important, for example evacuation assessments, the use of FDS as a coupled hybrid model may not have given accurate predictions.

To resolve this issue and to fulfil objective two of this thesis, the unsteady transport of mass and energy through the HVAC submodel has been developed by the authors and implemented within FDS version 6.5.3. This addition enables designers to use the coupled hybrid modelling method to effectively expand the domain of their calculation whilst still being able to deliver results to the stakeholder team within a reasonable and expected time frame.

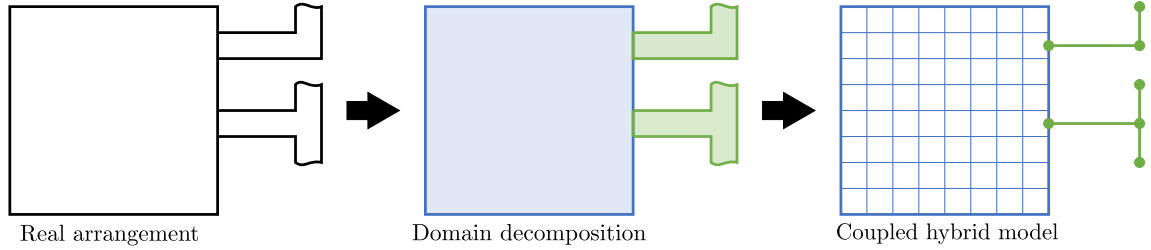


Figure 1: Domain decomposition.

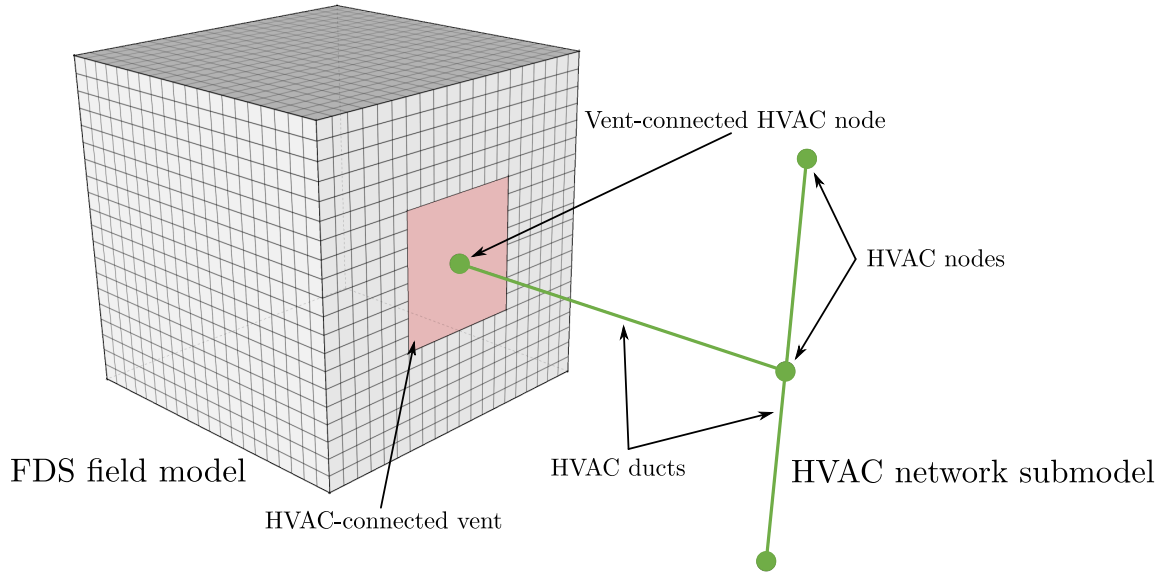


Figure 2: Primary components of coupled hybrid model within FDS.

2 Description of the existing HVAC submodel

2.1 General description

The new transient transport subroutine builds upon the existing HVAC submodel. The coupled hybrid model, being formed of the coupling of the FDS 3D field solver and the HVAC 1D network solver, can be used to solve the boundary value problem posed by a user-defined total domain incorporating various 3D and 1D geometries and boundary conditions. A non-overlapping domain decomposition method is used to form the subdomains of the two coupled submodels as shown in Figure 1.

Only a brief description of the previously existing HVAC submodel is provided here, the interested reader is referred to the FDS Technical Reference Guide [14]. The HVAC submodel is a 1D hydrodynamic network model which comprises a domain of connected ducts and nodes. The 1D network submodel exchanges information with the FDS field domain at special vent-connected HVAC nodes. Figure 2 presents a sketch of the coupled hybrid model.

Nodes have no volume and the submodel solves the following nodal conservation equations of mass and energy:

$$\sum_j \rho_j u_j A_j = 0 \quad (1)$$

$$\sum_j \rho_j u_j A_j h_j = 0 \quad (2)$$

And the conservation equation of momentum in a duct:

$$\rho_j L_j \frac{du_j}{dt} = (p_i - p_k) + (\rho g \Delta z)_j + \Delta p_j - \frac{1}{2} K_j \rho_j |u_j| u_j \quad (3)$$

The subscripts i , k , and j denote upstream node, downstream node and duct respectively. The first term on the right-hand side of the momentum equation is the pressure difference between the upstream and downstream nodes, the second term is the hydrostatic pressure head, the third term is a pressure increase source (e.g. a fan), and the fourth term is the pressure losses due to wall friction and minor losses (e.g. bends and fittings).

The following discretisation is used for the solution of the momentum equation which is non-linear with respect to velocity:

$$u_j^{n+1} = u_j^n \frac{\Delta t^n}{\rho_j L_j} \left((\tilde{p}_i^n - \tilde{p}_k^n) + (\rho g \Delta z)_j^n - \Delta p_j^n - \frac{1}{2} K_j \rho_j (|u_j^{n-} + u_j^{n+}| u_j^n - |u_j^{n+}| u_j^{n-}) \right) \quad (4)$$

The $n+$ and $n-$ superscripts denote, respectively, the prior iteration value and either the prior iteration value or zero if flow reversal has occurred. This is carried out to linearise the flow losses in a duct by avoiding large changes in K during flow reversal if the forward and backward losses are very different.

Node pressures are expressed as \tilde{p}_i (not p_i) because they are extrapolated pressures based upon the rate of pressure change during the previous time step. This is because the pressure solution of vent-connected nodes is based upon mass and energy flows predicted by the HVAC submodel and the FDS hydrodynamic solver. If the node is an internal node then the solution for the actual pressure is closed.

If convergence checks of mass conservation or velocity change fail, the solution for the momentum is re-iterated with a new extrapolated node pressure.

2.2 Boundary conditions at coupling location

2.2.1 Boundary conditions within the HVAC subdomain

There are two types of boundary condition required to solve the boundary value problem on the HVAC subdomain. Flow into the HVAC subdomain and flow out of the HVAC subdomain. Where the two types of boundary condition occur are represented in Figure 3.

The upstream quantities are used when updating the duct nodes. For flow into the HVAC subdomain (boundary condition type 1 in Figure 3) quantities are populated using data collected from the FDS domain and for flows out of the HVAC subdomain (boundary condition type 2 in Figure 3) quantities are populated using 1D data from the connected HVAC ducts.

For flow into the HVAC subdomain (boundary condition type 1 in Figure 3) information is required to be transferred from the FDS domain to the HVAC subdomain. This is a reverse “defective boundary condition” [15] and hence the 2D vent data from FDS which is connected to the vent-connected HVAC node must be reduced to 1D data. The density, species, enthalpy (based upon adjacent gas phase temperatures and species concentration), and temperatures are summed and averaged from gas cells adjacent to the HVAC-connected vent.

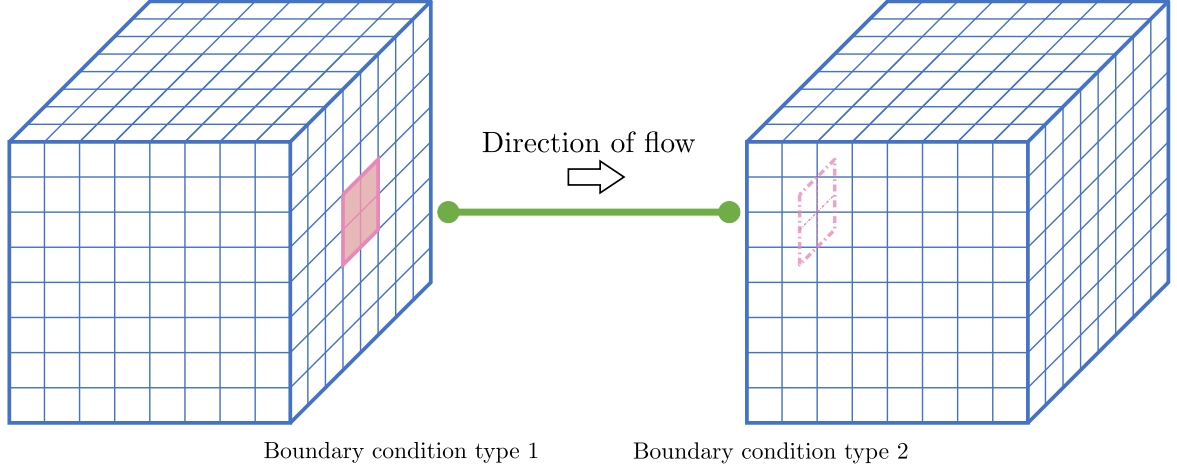


Figure 3: Two different types of coupling boundary condition within model.

$$\rho_i = \frac{\sum_{g \in V} \rho_g A_g}{\sum_{g \in V} A_g} \quad (5)$$

$$Y_{\alpha,i} = \frac{\sum_{g \in V} Y_{\alpha,g} A_g}{\sum_{g \in V} A_g} \quad (6)$$

$$p_i = \frac{\sum_{g \in V} p_g A_g}{\sum_{g \in V} A_g} \quad (7)$$

$$h_i = \frac{\sum_{g \in V} c_p(T_g, Y_g) T_g A_g}{\sum_{g \in V} A_g} \quad (8)$$

$$T_i = \frac{\sum_{g \in V} T_g A_g}{\sum_{g \in V} A_g} \quad (9)$$

The subscript i denotes duct nodes, g gas cells and V is the set of gas cells adjacent to the FDS vent which is connected to the vent-connected HVAC node (i). The summed and averaged temperature (T_i) may not correspond to the summed and averaged enthalpy (h_i) as there may be a variation in specific heat due to temperature and species across the gas cells adjacent to the FDS vent ($g \in V$) which is connected to the vent-connected HVAC node (i). The initial average temperature is therefore iterated to converge with the temperature equating to the average enthalpy, using the following Newton-Raphson root finding loop:

$$T_i^{k+1} = T_i^k + \frac{\left(h_i - h(T_i^k, Y_{\alpha,i}^k) \right)}{\left(c_p(T_i^k, Y_{\alpha,i}^k) + T_i^k \frac{\Delta c_p(T_i^k, Y_{\alpha,i}^k)}{\Delta T_i^k} \right)} \quad (10)$$

Where $h(T_i^k, Y_{\alpha,i}^k)$ is the enthalpy as output by the averaged temperature and the area-averaged species concentrations in the vent-connected HVAC node at that iteration. The density, species, and pressure of the vent-connected HVAC node is adopted as the averaged quantities in Equation 5 to 7, the temperature is adopted as the converged solution from Equation 10, and the specific heat of the vent-connected HVAC node is populated as:

$$c_{p_i} = \frac{h(T_i, Y_{\alpha,i})}{T_i} \quad (11)$$

For flow from the HVAC subdomain to the FDS domain (boundary condition type 2), the population of vent-connected duct node values is a trivial population using 1D duct quantities.

2.2.2 Boundary conditions within the FDS field domain

Again there are two types of boundary condition within the FDS field domain. When the flow is from the FDS field domain (boundary condition type 1 in Figure 3) and when flow is into the FDS field domain (boundary condition type 2 in Figure 3). The coupling boundary conditions within the FDS field domain are represented by 2D wall vents which are connected to vent-connected HVAC nodes. Vent wall cell quantities are adopted based upon upstream data (i.e. from the FDS field domain for coupling boundary condition type 1 and from the HVAC subdomain for coupling boundary condition type 2).

For coupling boundary condition type 1 (flow out of the FDS field domain) the wall vent cell quantities are generally populated using the adjacent gas cell quantities and the perpendicular velocity is output using the mass flux in the connected HVAC duct.

$$T_w = T_g \quad (12)$$

$$Y_{\alpha,w} = Y_g \quad (13)$$

$$\rho_w = \rho_g \quad (14)$$

$$u_w = \frac{\dot{m}_j''}{\rho_w} \quad (15)$$

Where the mass flux in the duct \dot{m}_j'' is output:

$$\dot{m}_j'' = \frac{u_j A_j \rho_j}{A_v} \quad (16)$$

For coupling boundary condition type 2 (flow into the FDS field domain) the wall vent cell quantities are populated using the spatially averaged quantities from the vent-connected HVAC node within the HVAC subdomain. Coupling boundary condition type 2 within the FDS field domain is a defective boundary condition. The problem is mathematically ill-posed and the input data (single dimensional averaged velocity) is scarce compared to the required output data (three-dimensional spatially resolved velocity). An interpolation method must be used to address these defective boundary conditions.

For other applications of a coupled hybrid fluid solver the coupling boundary conditions span two entire dimensions of the subdomains. For example, Blanco et al. [16] and Colella et al. [17] use coupled hybrid fluid models for simulation of blood vessel networks and tunnel networks respectively. In these cases the coupling boundary conditions span both the y and z dimensions. In these cases it is reasonable to assume that the spatial distribution of quantities such as the velocity and the density on the coupling boundary condition could affect the overall solution. For these applications, the treatment of the defective boundary condition may be critical to the meaningful solution of the boundary value problem being solved on the decomposed hybrid domain. In these cases advanced interpolation methods such as the Lagrange multiplier method, Nitsche's method [18], and Schur's method [19] have been adopted within the literature.

The coupling boundary conditions within the FDS field model (being the HVAC-connected vents) will typically occupy only a fraction of the overall dimensions of the domain. Within the parameter

space which is the subject of this work, these interpolation methods are concluded to be too expensive to justify their use. The speed reduction is not seen as justifiable for the majority of code users. If the coupled hybrid model is further expanded to another parameter space then the treatment of the defective boundary conditions will be addressed. The wall vent cell quantities are populated using a linear distribution model based upon quantities from the upstream HVAC subdomain.

$$T_w = T_i \quad (17)$$

$$\dot{m}''_{\alpha,w} = \dot{m}''_j Y_{\alpha,i} \quad (18)$$

$$u_w = \frac{\dot{m}''_j}{\rho_w} \quad (19)$$

$$Y_{\alpha,w} = \frac{\dot{m}''_{\alpha,w} + \frac{2\rho_w D_\alpha Y_{\alpha,g}}{\delta n}}{u_w \rho_w + \frac{2\rho_w D_\alpha}{\delta n}} \quad (20)$$

$$\rho_w = \frac{\bar{p}\bar{W}_w}{RT_w} \quad (21)$$

Where mass flux in the duct \dot{m}''_j is per Equation 16. To ensure consistency between the species mass fraction, density, and velocity, Equations 19 to 21 are solved iteratively using the iterating method given in Equations 22 to 25.

$$u_w^{k+1} = \frac{\dot{m}''_j}{\rho_w^k} \quad (22)$$

$$(\rho_w D_\alpha)^{k+1} = (\rho_w D_\alpha)^k \frac{\rho_w^k}{\rho_w^{(k-1)^*}} \quad (23)$$

$$Y_{\alpha,w}^{k+1} = \frac{\dot{m}''_{\alpha,w} + \frac{2(\rho_w D_\alpha)^{k+1} Y_{\alpha,g}}{\delta n}}{u_w^{k+1} \rho_w^k + \frac{2(\rho_w D_\alpha)^{k+1}}{\delta n}} \quad (24)$$

$$\rho_w^{k+1} = \frac{\bar{p}\bar{W}_w (Y_{\alpha,w}^{k+1})}{RT_w} \quad (25)$$

Where $(k-1)^*$ is data either from the previous iteration or the previous time step if it is the first iteration.

2.3 Pertinent limitations of the pre-existing HVAC submodel

The pre-existing HVAC network submodel, prior to FDS version 6.5.3, did not account for transient transport of mass, species, or energy. This omission had two main implications for its use as part of a coupled hybrid model. Firstly, there was no mass, species, or energy storage within the HVAC network subdomain. Thus any mass, species, or energy within the portion of the total domain being simulated using the HVAC network submodel was ignored and did not form part of the total domain calculation. Secondly, the coupled hybrid model implementation did not account for the time taken for mass, species and energy to be transported through the HVAC network subdomain. Any mass, species or energy passing into the HVAC network subdomain was instantaneously moved to the connected FDS field domain(s).

3 New unsteady transport subroutine

3.1 Conservation equations and numerical solution

A new transient transport subroutine has been developed which is an augmentation to the existing HVAC network submodel and addresses the limitations described in Section 2.3. The new subroutine uses the

existing nodal conservation equations for mass and energy, duct conservation equation for momentum. The HVAC transient transport subroutine is an explicit Runge-Kutta method [20] conservation of species and energy using a finite difference Euler method [21] with a Godunov upwinding scheme [22]. In a typical HVAC system, as velocities in the ducts are relatively high, transport due to advection is expected to greatly outweigh that due to diffusion. Based upon this assumption of a high Péclet number the subroutine accounts for advective transport only (i.e. no diffusive transport). The analytical form of the conservation equation solved:

$$\frac{\rho \partial \phi}{\partial t} = -u \frac{\rho \partial \phi}{\partial x} \quad (26)$$

The ducts are discretized into cells with conserved variables (species mixture, specific heat, temperature, and density) being located at cell centres. The numerical discretization used to solve the partial differential equation is:

$$(\widetilde{\rho\phi})_c^{n+1} = (\widetilde{\rho\phi})_c^n - \frac{\Delta t}{\Delta x} (\rho u)_j^n (\bar{\phi}_{c+\frac{1}{2}}^n - \bar{\phi}_{c-\frac{1}{2}}^n) \quad (27)$$

Where $(\rho u)_j^k$ is the mass flow within the duct and tilde and bar represent cell centred and cell face quantities respectively. A Godunov pure upwinding scheme is used to define the cell face values:

$$(\widetilde{\rho\phi})_c^{n+1} = (\widetilde{\rho\phi})_c^n - \frac{\Delta t}{\Delta x} (\rho u)_j^n (\tilde{\phi}_c^n - \tilde{\phi}_{c-1}^n) \quad (28)$$

The Courant-Friedrichs-Lewy (CFL) condition for the Godunov scheme is $\Delta t \leq \frac{\Delta x}{2u}$. To ensure stability for the HVAC transient transport subroutine, the time step used in the subroutine could drop lower than the FDS time step. To maintain the CFL condition, the subroutine takes sub-steps of the FDS time step via the least integer of the FDS time step divided by the CFL time step.

A second CFL condition on the solver is:

$$\Delta t \leq \frac{\sum_{c \in j} m_c}{\dot{m}'_j A_j} \quad (29)$$

Where Δt is the solver time step, the term in the numerator is the sum of the masses within all cells in a duct, \dot{m}'_j is the mass flow rate in the duct, and A_j is the area of the duct. The physical meaning of this limit is to ensure that the mass flowing out of a duct within a transient solver time step is not greater than the content of mass in the duct. If this CFL is breached then a sub-step time step is created for the transient solver (which is less than the global time step).

Energy is conserved as a single variable. To separate the specific heat and the temperature, and hence be able to update the cell centred variables, the Newton-Raphson method, as described in Equation 30, is used to iterate on the cell temperature T_c . A maximum iteration number of ten or a variation in T_c^{k+1} and T_c^k of less than 0.05 % is used.

$$T_c^{k+1} = T_c^k + \frac{(c_p T)_c^0 - h_c^{k+1}(T_c^k, Y_c)}{c_{p_c}^{k+1}(T_c^k, Y_c) + T_c^k \cdot \left[\frac{\delta c_p}{\delta T}(Y_c) \right]_c^{k+1}} \quad (30)$$

Where $(c_p T)_c^0$ is the initial enthalpy estimate from the solution of Equation 28 and $\left[\frac{\delta c_p}{\delta T}(Y_c) \right]_c^{k+1}$ is an estimate of the species-dependent variation in specific heat due to temperature. This estimated gradient is output using a discrete interpolation across a 1 K temperature range at the current time step temperature using a species-specific pre-populated $c_p(T)$ lookup table. Following the iteration on cell temperature, the cell specific heat is:

$$c_{p_c} = \frac{h(T_c, Y_c)}{T_c} \quad (31)$$

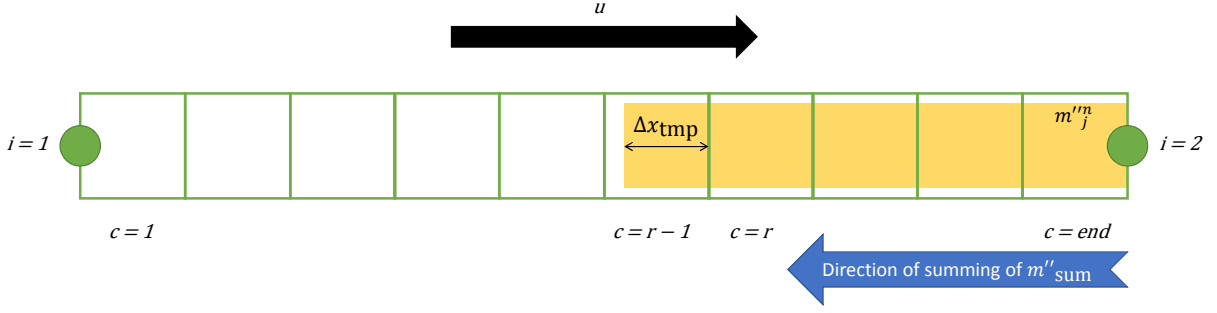


Figure 4: Backward summing of mass to locate and dimension temporary duct cell.

3.2 Checking flow through an HVAC node

With the exception of the updating of the conservation equations within the transient solver, the HVAC network submodel time step matches the FDS field model time step. There is potential for a non-integer number of cells' content to flow through a node from connected ducts within a time step. This is not acceptable as the HVAC submodel uses total flows of mass, energy and species passing through HVAC nodes for velocity and mass convergence checks, and for separating quantities from conserved variables. For example, if duct cells had a length of 0.1 m, the velocity in the duct was 3.5 m/s and the global time step was 0.1 s then the variable advected within a time step would be contained in 3.5 cells. When computing the total flow passing through a node, this non-integer amount of cell content should be calculated.

The spatial end of the volume of mass which will be advected within a time step is first located. This is carried out by summing the cumulative mass passing through duct cells in that time step (m''_{sum}), from the end cell backwards, and comparing this to the total mass passing through the duct in that time step output from the steady state HVAC solver (m''_j).

The duct cell within which the end of the advected mass falls within is defined as cell $r - 1$. Hence, a new temporary cell size (Δx_{tmp}) is output. This temporary cell size is dimensioned such that the contents of all the previously backward-summed cells (from the final cell to the r^{th} cell) and the temporary cell is equal to the total duct mass flux in that time step (m''_j). This is described in Equation 32 and Figure 4.

$$\Delta x_{\text{tmp}} = \frac{m''_j - \sum_{r \leq c \leq \text{end}} m''_c}{\rho_c} \quad (32)$$

This temporary cell size is then used to compute the total variable flowing from a duct through a node. For example, Equation 33 gives the computation of enthalpy flowing through a node i from all connected ducts j within a time step n .

$$h_i^n = \sum_j \left(\sum_{r \leq c \leq \text{end}} (\rho_c c_p T \Delta x)_c + \rho_c c_p T_c \Delta x_{\text{tmp}} \right) A_j \quad (33)$$

3.3 Initialisation

A duct in the HVAC subdomain is defined by a pair of nodes. Duct runs are sets of ducts and nodes which are connected to one another directly by way of the HVAC network subdomain. When initialising the conditions in a duct run, with transient transport enabled, the user has two options: use the conditions of the lowest numbered node in the duct run (DUCT_INTERP_TYPE=NODE1) or use the conditions of the highest numbered node in the duct run (DUCT_INTERP_TYPE=NODE2). There is a third developer option (linear interpolation) which is used only for verification cases.

Before initialisation of the HVAC network model, a bespoke network clustering algorithm is used to group connected ducts and duct nodes into individual duct runs. The original clustering algorithm starts at the first node, loops through all connected ducts and tags all numerically downstream nodes as connected to the initial node. This process is looped over all nodes until all nodes and ducts are assigned

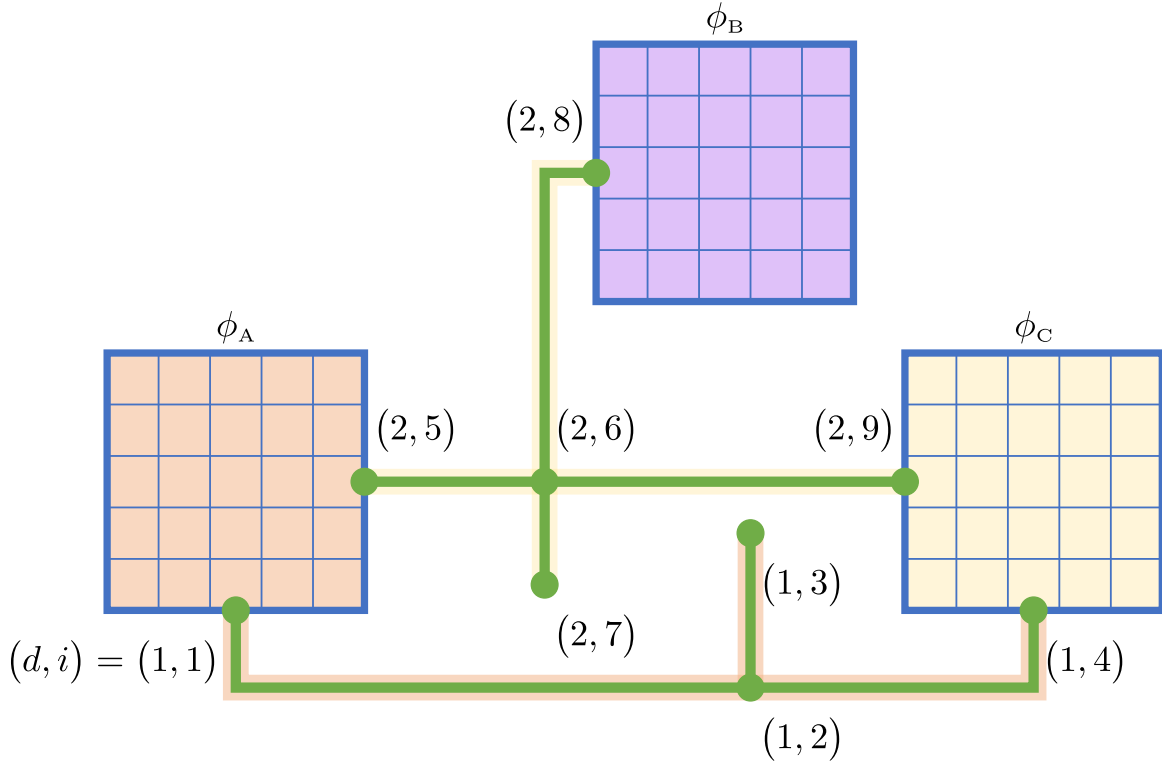


Figure 5: Two methods of interpolation for duct runs. Duct run $d = 1$ and $d = 2$ are initialised with quantities ϕ_A (orange) and ϕ_C (yellow) respectively

to a duct run. With duct runs known, the initialising can then proceed to propagate the quantities of the relevant vent-connected HVAC node through all elements of the duct run set (j ducts, i nodes, and c cells) according to the user selected initialisation option.

An example is given in Figure 5, which presents a coupled hybrid decomposed domain comprising three FDS field domains (A , B and C) and two HVAC subdomain duct runs ($d = 1$ and $d = 2$). The three FDS field domains A , B and C are filled with quantities ϕ_A , ϕ_B , and ϕ_C respectively. The user has selected (DUCT_INTERP_TYPE=NODE1) for duct run $d = 1$ and (DUCT_INTERP_TYPE=NODE2) for duct run $d = 2$. The lowest numbered node in duct run $d = 1$ is $i = 1$ which is connected to FDS field domain A . Therefore the entire duct run $d = 1$ is initialised with quantities ϕ_A (orange). The highest numbered node in duct run $d = 2$ is $i = 9$ which is connected to FDS field domain C . Hence the duct run $d = 2$ is initialised with quantities ϕ_C (yellow).

4 Verification

Numerical verification of the HVAC unsteady transport subroutine in accordance with ASTM E 1355 [23] has been carried out. Verification is carried out using FDS release version 6.7.0. All cases are available on the FDS GitHub repository (<https://github.com/firemodels/fds/tree/master/Verification/HVAC>).

The HVAC unsteady transport subroutine is enabled by setting HVAC_MASS_TRANSPORT=.TRUE. on the &MISC line in the input file.

Unless otherwise stated, the general verification test case comprises two 0.5 m^3 FDS field model compartments connected, in some manner, by an HVAC network subdomain. The general arrangement is described in Figure 6. The left and right compartments are initialised with species 1 and species 2 respectively which have identical transport and thermophysical properties. Both species have an initial density of 1 kg/m^3 . The duct(s) have a cross sectional area of 0.01 m^2 and a flow rate of $0.01\text{ m}^3/\text{s}$ (an ideal velocity of 1 m/s).

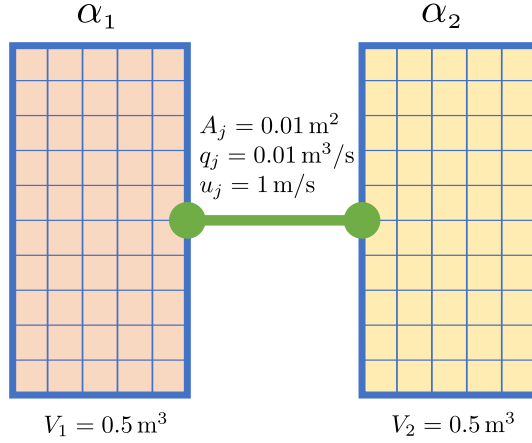


Figure 6: General verification case. Two FDS field model compartments, initialised with species 1 and 2, connected by an HVAC subdomain.

4.1 Numerical convergence study

The HVAC transient transport subroutine is an Euler method with Godunov upwinding scheme. This method is formally first-order accurate in space and should exhibit l_1 -norm error decay rates of $\mathcal{O}(\Delta x)$ for a non-discontinuous solution. A convergence study is undertaken to demonstrate that the adopted numerical method exhibits the expected spatial error decay.

The two FDS field model compartments are connected with a single 1 m long HVAC submodel duct which is initialised using linear interpolation between the upstream and downstream duct node. In this manner the mass fraction of species 1 linearly decreases from 1 to 0 kg/kg along the duct. When the species 1 mass fraction at the downstream node is examined, its value is expected to increase linearly from 0 kg/kg to 1 kg/kg between 0 s and 1 s and then to remain at 1 kg/kg until the end of the simulation. The mass fraction of species 1 at the downstream duct node is examined and compared to the analytical result for a range of duct cell numbers (20, 40, 80, 160 and 320). The time step is fixed to satisfy the CFL of the case cell size; this ensures that the $\frac{\Delta x}{\Delta t}$ ratio is fixed for each case.

Figure 7 shows the mass fraction of species 1 at the downstream duct node for all cases and the analytical solution. The figure illustrates the mass fraction of species 1 starting at zero and then linearly increasing due to the initial conditions in the duct. At 1 s the mass fraction reaches its maximum and remains at this value until the end of the simulation. The figure illustrates that at lower cell counts (blue line) there is increased numerical diffusivity and that, for higher cell counts (cyan line), the numerical solution converges towards the analytical solution (black dashed line). Figure 8 presents the L1-norm error decay and demonstrates the numerical solution decays at $\mathcal{O}(\Delta x)$ towards the exact solution for decreasing cell size Δx as expected.

4.2 Species transport time

A single 10 m long HVAC submodel duct connects the two FDS field model compartments. The duct is initialised using data from the right duct node (i.e. species 2). Species 1 mass fraction at the downstream duct node is expected to start and remain at 0 kg/kg until 10 s and then instantaneously increase to 1 kg/kg as the content of the left FDS field model compartment has passed through the duct and reached the left node. The exact solution and the numerical solution are presented in Figure 9. The figure demonstrates that the expected transport time for species 1 is observed. The slightly non-discontinuous species concentration (i.e. not a step function at $t = 10$ s) is due to numerical diffusion. This numerical diffusion is due to the Godunov scheme used and has been shown in Section 4.1 to decrease as $\mathcal{O}(\Delta x)$.

4.3 Mass conservation

The two FDS field model compartments are connected by two HVAC submodel ducts, A and B, being 5 m and 10 m long respectively. Duct A is initialised with species 1 and has a flow from left to right and

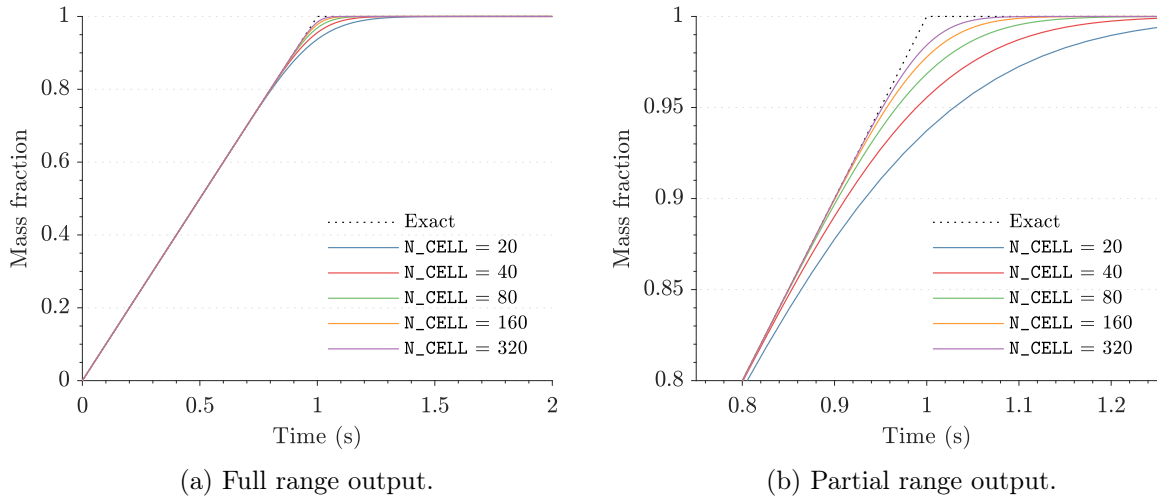


Figure 7: Exact and numerical solutions for node 2 mass fraction, showing convergence towards exact solution.

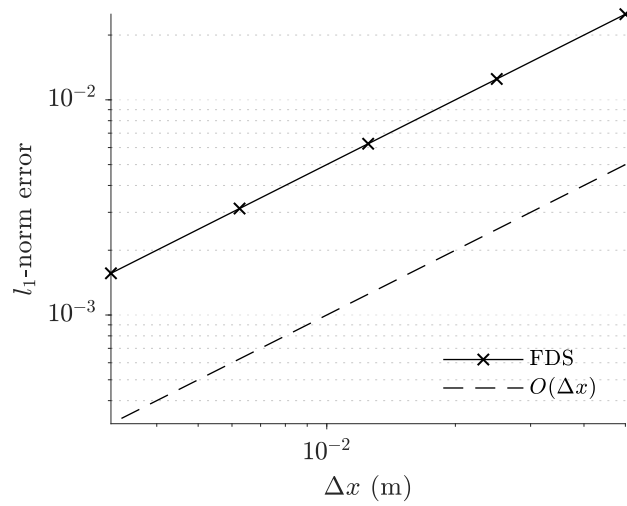


Figure 8: l_1 -norm error between the numerical solutions and the exact solution, showing $\mathcal{O}(\Delta x)$ error decay.

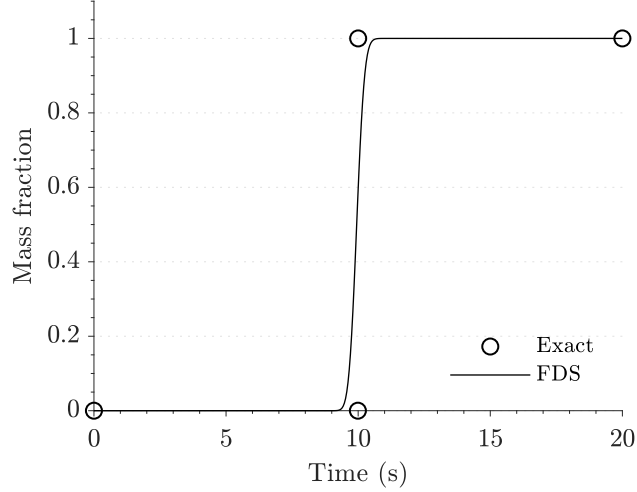


Figure 9: Mass fraction of species 1 at the downstream node 2 for transport time verification case.

duct B is initialised with species 2 and has a flow from right to left. The mass of species 1 and 2 in the total hybrid domain are:

$$\sum_{\Omega_{\text{hybrid}}} m_1 = m_{1,\text{left}} + m_{1,\text{duct A}} = 0.5 \text{ kg} + 0.05 \text{ kg} = 0.55 \text{ kg} \quad (34)$$

$$\sum_{\Omega_{\text{hybrid}}} m_2 = m_{2,\text{right}} + m_{2,\text{duct B}} = 0.5 \text{ kg} + 0.2 \text{ kg} = 0.7 \text{ kg} \quad (35)$$

Therefore, 0.05 kg (0.022 kg of species 1 and 0.028 kg of species 2) and 0.2 kg (0.088 kg of species 1 and 0.112 kg of species 2) of gas mixture is expected to be stored within the HVAC subdomain in ducts A and B respectively. Therefore the remaining 1 kg of gas mixture (0.44 kg of species 1 and 0.56 kg of species 2) is expected to be within the FDS field domain at equilibrium.

Figure 10 shows the total masses of species 1 and 2 within the FDS field domain for the verification case. The figure illustrates the two species each starting at the initial conditions of 0.5 kg, gas phase mixing and establishment of equilibrium. As expected, species 1 and 2 come to equilibrium at 0.44 kg and 0.56 kg respectively (their total hybrid domain mass ratio of 0.44 : 0.56).

4.4 Branching ducts

This verification case checks that the transient transport solution is correct for an HVAC subdomain which incorporates a bifurcating duct run. The schematic of the case is presented in Figure 11. The two FDS field compartments are connected by an HVAC network subdomain comprising a single 5 m feed duct (duct 0) which branches into two ducts (ducts A and B) at a tee with both ducts A and B discharging to the right compartment. Ducts A and B each have a cross-sectional area of 0.005 m^2 , half that of the feed duct 0. Both ducts A and B will therefore both have a velocity of 1 m/s. Duct A has a length of 5 m and duct B has a length of 10 m. The HVAC subdomain is initialised using data from the right FDS field compartment (species 2).

Based on the duct lengths and a constant velocity of 1 m/s the species 1 mass fraction at outlet A and B is expected to increase from 0 kg/kg to 1 kg/kg at 10 s and 15 s respectively. Exact and numerical solutions are presented in Figure 12. The figure illustrates that it takes 10 s for the upstream species 1 to reach the discharge node of duct A and 15 s for the upstream species 1 to reach the discharge node of duct B as expected. The slight variation is related to numerical diffusion inherent in the first-order scheme.

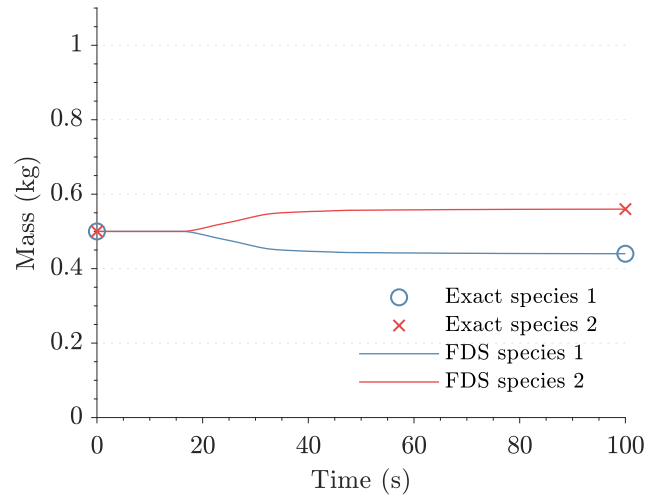


Figure 10: Total masses of species 1 and 2 in the FDS field domain for the mass conservation 2 verification case.

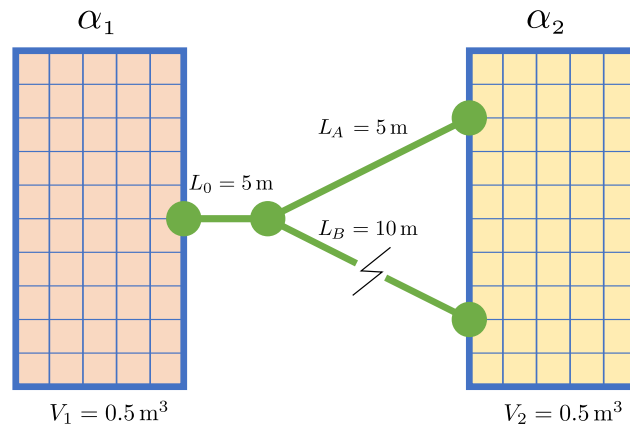


Figure 11: Branching ducts verification case. Velocity through HVAC subdomain is constant as ducts A and B have a cross-sectional area half that of duct 0.

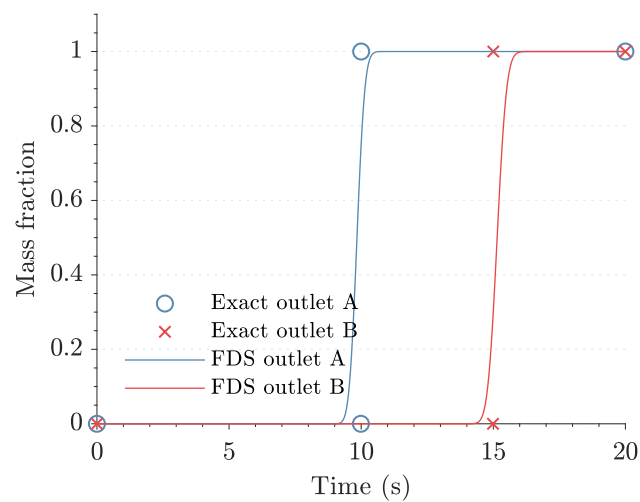


Figure 12: Mass of species 1 at the downstream nodes A and B. Transport time to the discharge node of duct A and B is expected to be 10 s and 15 s respectively.

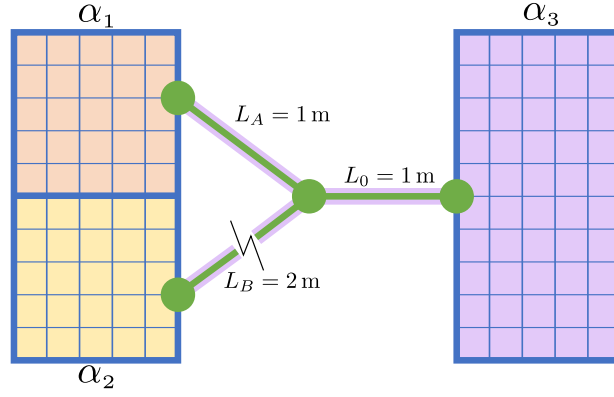


Figure 13: Combining ducts verification case. Velocity through HVAC subdomain is constant as ducts A and B have a cross-sectional area half that of duct 0.

4.5 Combining ducts

This verification case checks the combining of HVAC ducts at nodes and the correct mixing of gas species. The schematic of the case is presented in Figure 13. The left FDS field compartment is separated into two sub-compartments, A and B. FDS field sub-compartments A and B are initialised with species 1 and 2 respectively. An inlet vent is located in both sub-compartments A and B. The inlet vents in sub-compartment A and B are connected to two separate HVAC ducts (duct A and B), of lengths 1 m and 2 m respectively, which combine at an internal tee. A single HVAC duct (duct 0), with a length of 1 m, connects this tee to the right FDS field compartment where it discharges to a single outlet vent. Ducts A and B each have a cross-sectional area of 0.005 m^2 , half that of the feed duct 0. Both ducts A and B will therefore both have a velocity of 1 m/s . The right compartment and the duct network is initialised with species 3.

The species mass fractions at the downstream outlet duct node are expected to be a species 3 mass fraction of 1 kg/kg for 2 s, a species 1 and 3 mass fraction of 0.5 kg/kg each from 2 s to 3 s and a species 1 and 2 mass fraction of 0.5 kg/kg each from 3 s until the end of the simulation. The exact solution and the numerical solution is presented in Figure 14. The figure shows that species 3 starts and remains at 1 kg/kg for 2 s as the initial contents of the HVAC subdomain flows out of the outlet node. At 2 s the species from FDS field sub-compartment A and the remaining initial species from the longer HVAC subdomain duct B flows out of the outlet node. At 3 s the species from FDS field sub-compartment B reaches the outlet node and the mass fraction is split between the species from the two upstream FDS field sub-compartments (no initial species remains in the ducts).

4.6 Energy conservation and pressure

This verification case checks that gas phase energy is conserved within the total hybrid domain and that pressure drop down an HVAC duct is correctly computed. The left FDS field compartment is initialised with a temperature of $100 \text{ }^\circ\text{C}$, the right FDS field compartment remains at ambient $20 \text{ }^\circ\text{C}$. The total hybrid domain is initialised with a single species. The species has a specific heat of $1 \text{ kJ}/(\text{kg K})$. The pressure in both FDS field compartments is ambient (101325 Pa). All surfaces are set as adiabatic. The FDS field compartments are connected by two separate HVAC ducts, ducts A and B, both with a length of 1 m. Duct A has a specified flow from left to right with a velocity of 1 m/s , duct B has no defined flow and a minor losses coefficient $K_{\text{minor}} = 2$. HVAC duct A and B are initialised using gas data from the left and right FDS field compartments respectively (i.e. duct A has a gas temperature of $100 \text{ }^\circ\text{C}$ and duct B of ambient).

The enthalpy in the FDS field domain is expected to be 293.15 kJ in Equations 37 to 38. This value should remain constant. Figure 15 presents the exact and numerical solution for the enthalpy within the FDS field domain. The figure demonstrates that energy is conserved within the coupled hybrid model incorporating gases at different temperatures, with different enthalpies, mixing within the total domain.

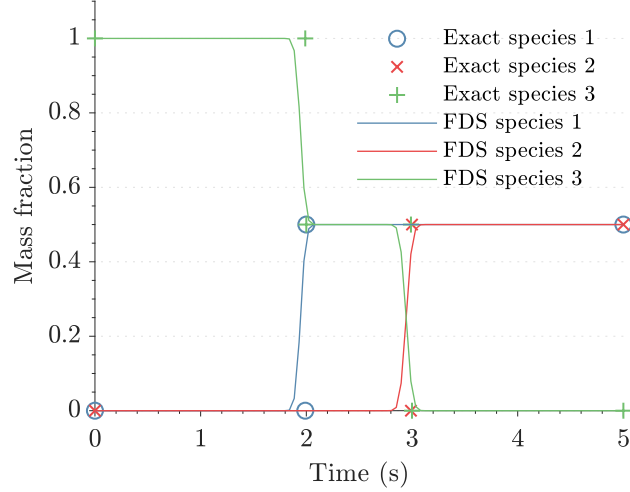


Figure 14: Species 1, 2 and 3 mass fraction at the outlet node into the right FDS field compartment. Initially flow comprises only species 3, then a 50 : 50 mix of species 1 and 3 and finally a 50 : 50 mix of species 1 and 2.

$$h_{\text{field}} = c_p \frac{V_{\text{field}}}{2} (T_{\text{left}} \rho_{\text{left}} + T_{\text{right}} \rho_{\text{right}}) \quad (36)$$

$$h_{\text{field}} = 1 \text{ kJ}/(\text{kg K}) \cdot \frac{1 \text{ m}^3}{2} (373.15 \text{ K} \cdot 0.786 \text{ kg}/\text{m}^3 + 293.15 \text{ K} \cdot 1 \text{ kg}/\text{m}^3) \quad (37)$$

$$h_{\text{field}} = 293.15 \text{ kJ} \quad (38)$$

To check the pressure drop along the length of duct B, first the enthalpy within the total hybrid domain in Equations 40 to 42 is calculated to enable the output of the steady state temperature and density at equilibrium.

$$h_{\text{total}} = h_{\text{field}} + h_{\text{network}} \quad (39)$$

$$h_{\text{total}} = h_{\text{field}} + c_p \frac{V_{\text{network}}}{2} (T_A \rho_A + T_B \rho_B) \quad (40)$$

$$h_{\text{total}} = 293.15 \text{ kJ} + 1 \text{ kJ}/(\text{kg K}) \cdot \frac{0.2 \text{ m}^3}{2} (373.15 \text{ K} \cdot 0.786 \text{ kg}/\text{m}^3 + 293.15 \text{ K} \cdot 1 \text{ kg}/\text{m}^3) \quad (41)$$

$$h_{\text{total}} = 351.78 \text{ kJ} \quad (42)$$

Next the equilibrium temperature is calculated. Finally the expected steady state pressure drop between the inlet and outlet node of duct B is calculated in Equation 46.

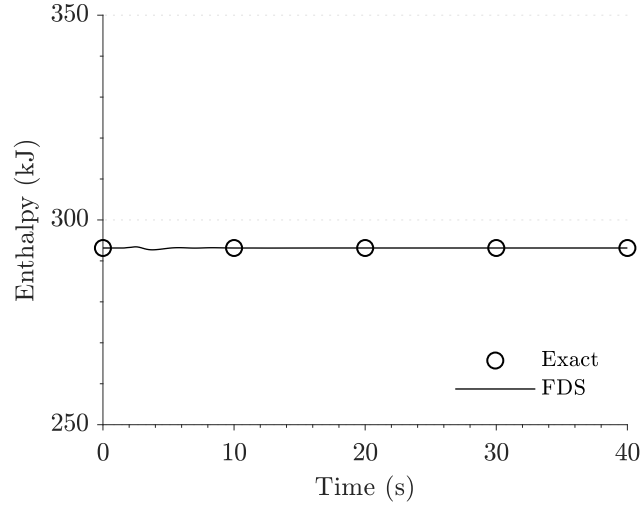


Figure 15: Enthalpy within the FDS field domain for the energy conservation and pressure verification case. Enthalpy is conserved for the gases at different temperatures mixing.

$$T_{SS} = \frac{h_{total}}{c_p m_{total}} \quad (43)$$

$$T_{SS} = \frac{351.78 \text{ kJ}}{1 \text{ kJ}/(\text{kg K}) \cdot 1.2 \text{ kg}} = 328.35 \text{ K} \quad (44)$$

$$\Delta p_B = \frac{K_{minor} \rho_{SS} u^2}{2} \quad (45)$$

$$\Delta p_B = \frac{2 \cdot 0.8928 \text{ kg}/\text{m}^3 \cdot 1 \text{ m}/\text{s}^2}{2} = 0.8928 \text{ Pa} \quad (46)$$

Where the subscript SS denotes steady state values. Figure 16 presents the pressure drop calculated by the HVAC network submodel down the length of duct B from the upstream node to the downstream node. The figure describes the initial transitory unsteady state wherein the gases at two temperatures and densities are mixing within the total hybrid domain. After this transitory state, steady state is established, wherein the gas temperature, density and duct velocity are at equilibrium, and the expected duct pressure drop is predicted.

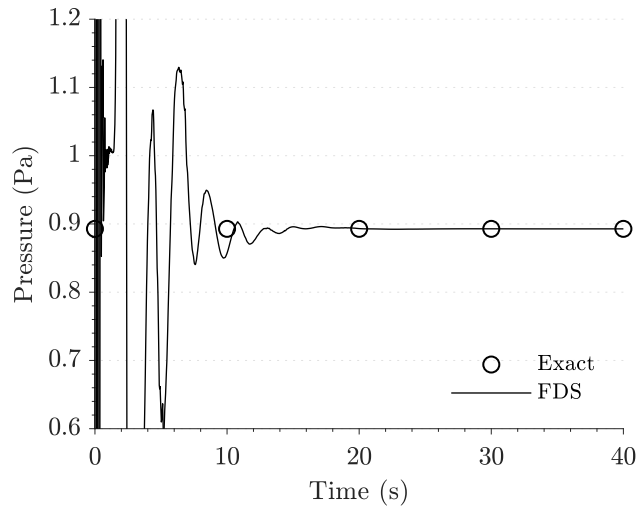


Figure 16: Pressure drop between the upstream and downstream HVAC nodes of duct B for the energy conservation and pressure verification case. After an initial transient stage, prior to equilibrium gas temperature and duct flow rate, the pressure drop down duct B is as expected.

5 Fire engineering test case example

To demonstrate the advantages of the new unsteady coupled hybrid modelling method implemented into FDS from version 6.5.3 onward a test case is presented representing a typical fire engineering assessment. The test case is designed to represent a two room arrangement where the rooms are connected only with a shared ventilation system. This is typical of an office building or hospital wards.

A fire will be modelled in the left room. The evolution of hot layer height, head height temperature, and head height visibility in proximity to the exit doors will be examined. These output quantities are typical of a fire engineering assessment for occupant evacuation. The calculation will be carried out for two cases; case 1, where `HVAC_MASS_TRANSPORT=.FALSE.`, and case 2, where `HVAC_MASS_TRANSPORT=.TRUE.`.

The rooms will be modelled within the FDS field domain and the ventilation system will be within the HVAC network subdomain.

5.1 Description of general arrangement of test case

Both rooms are 6 m wide, 9 m deep and 3 m high. Both rooms are provided with leakage to ambient at door locations at the back of the rooms. The leakage is located at the door sills and below the lintels and totals 0.02 m^2 per door. The walls are modelled as `INERT` (a Dirichlet boundary condition at a constant temperature of 20°C). The steady state heat release rate of the fire is 500 kW and starts at $t = 50 \text{ s}$. The fire is located at ground level, in the centre of the left room. Height height is defined as 2.1 m above finished floor [24].

All ventilation ducts are circular. The exhaust and supply ducts serving each room have a diameter of 0.2 m. The shared return duct has a diameter of 0.3 m. Duct cross-sectional areas are adopted to achieve duct velocities typical for office buildings (5 m/s to 10 m/s [25]). The set of two exhaust ducts and two supply ducts each have a length of 10 m. The shared return duct, which contains the mechanical ventilation fan, has a length of 100 m. Duct wall roughnesses are taken as 0.003 m, typical for aluminium ducts [26]. Minor loss coefficients for fittings and junctions are taken from the literature [27]. The ventilation fan has a maximum flow rate of $0.36 \text{ m}^3/\text{s}$ which approximately equates to an air change per hour of 4 (typical for office accommodation [28]). The exhaust vent in each room is orientated horizontally and located on the ceiling in the centre of the room. The supply vent in each room is orientated vertically and located on the rear wall of the room.

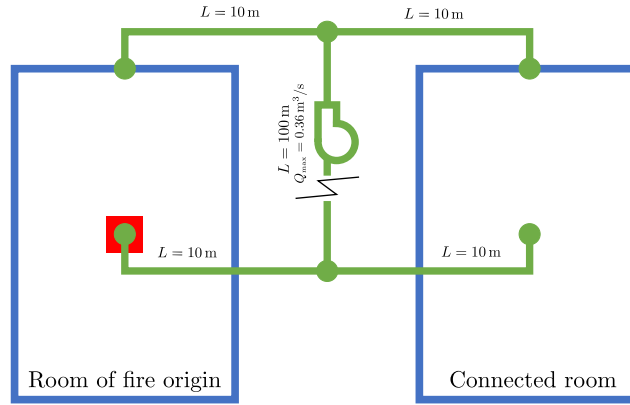


Figure 17: Plan of two room test case. The left room contains the fire and is connected to a non-fire room through a shared ventilation system.

5.2 Simulation and numerical parameters

The Deardorff turbulent viscosity model is used. A single-step, mixing-controlled combustion model is used. The adopted fuel is polyurethane with a soot yield of 0.1 kg/kg. A cell size of 0.1 m is adopted for this comparative analysis. A visibility factor of 3 is used.

5.3 Results

Key life safety quantities have been output in the vicinity of the exit doors in each of the two rooms. The exit doors have been nominally placed at the centre front of each room. The conditions are those expected to be experienced by occupants entering or queuing at the exit doors. This is a typical fire engineering methodology used to output the available safe egress time (ASET).

5.3.1 Hot layer height

The hot layer height in vicinity of the exit doors is examined. To output hot layer height a data reduction method must be used to reduce the three-dimensional field data to a single parameter called layer height (the interface between the hot upper layer and the cooler lower layer). Here the method proposed by Janssens [29] is used which has shown good agreement with experimental results.

Figure 18 presents the output for the two cases. Figure 18a illustrates that in case 1 the layer height in the connected room is predicted to drop very rapidly following that of the room of fire origin. This is because, with `HVAC_MASS_TRANSPORT=.FALSE.`, FDS does not predict the transport time required for gas phase quantities to move through the HVAC network domain. Whatever mass and energy is removed from the FDS field domain at the upstream vent is instantly transported to the downstream vent. The slight delay in the dropping of the hot layer (approximately 15 s is due to the requirement for smoke to flow out of the low level supply vent, rise to the ceiling, and start forming a hot layer. Figure 18b demonstrates that for case 2 the layer height in the connected room starts to drop approximately 50 s after that of the fire room. This is because case 2, with `HVAC_MASS_TRANSPORT=.TRUE.`, predicts the transient transport of mass and energy through the HVAC network subdomain.

The near-instantaneous dropping of the layer height in the connected room for case 1 would have drastic impact upon the fire engineering analysis, conclusions and requirements. For example, provisions related to occupant notification and evacuation (sizing of horizontal and vertical exits, and use of phased or simultaneous evacuation). The use of the coupled hybrid model within FDS version 6.5.2 or earlier (i.e. case 1) could lead to over-onerous and under-optimised fire engineering requirements.

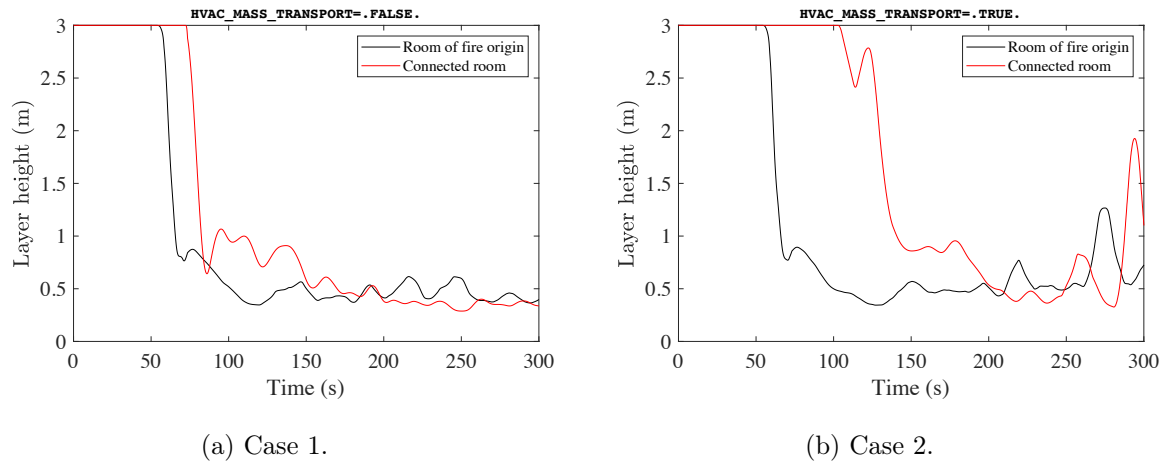


Figure 18: Hot layer height in proximity to the exit for the two cases.

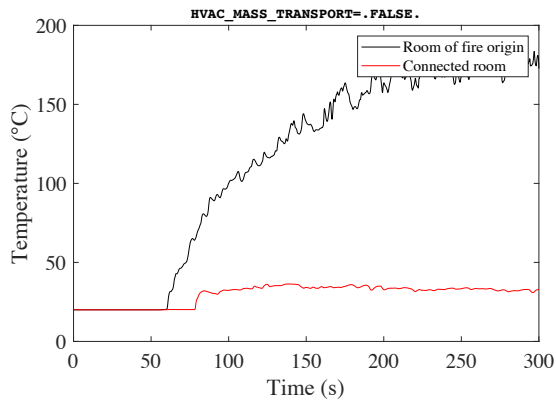
5.3.2 Head height temperature at exit

Figure 19 presents the head height temperature predictions within the fire and connected room for the two cases. It shows that the temperature at head height in the connected room in both cases does not rise greatly above ambient. For this assessment, temperature may not be the critical life safety criterion for occupants egressing the connected room (a value of 60°C is typically used [24]). However, Figure 19 does show two interesting and important differences between cases 1 and 2.

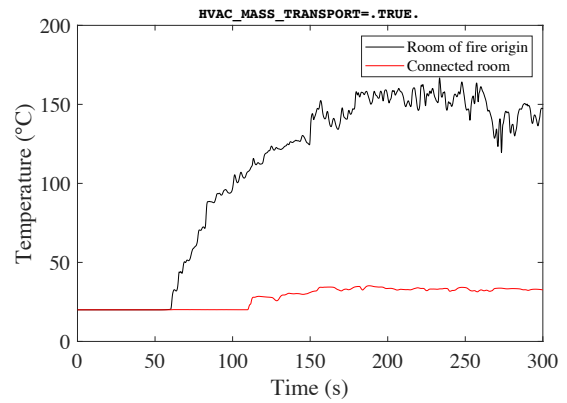
Firstly, Figure 19a illustrates that, for case 1, the increase in the predicted temperature at head height in the connected room increases soon after the predicted increase in temperature in the fire room. This is because there is no simulated transport time and all energy and mass is instantly moved from the fire room to the connected room. In comparison, Figure 19b demonstrates that for case 2 the expected delay in the increase in predicted head height temperature is predicted. This is because case 2 simulates the gas transport time through the ventilation system.

Secondly, Figure 19 shows a higher predicted head height temperature in the fire room for case 1 when compared to case 2. This is because case 1 ignores the presence of ambient temperature air within the ventilation system. Case 2 accounts for the volume of ambient gas within the ventilation system (which is initially within the HVAC network subdomain). In case 2, there is a volume of ambient air continuing to flow into the fire room from the ventilation system after a hot layer has formed within the connected room. This cooler air will mix with the hot gas layer in the fire room and reduce the predicted head height temperature in the fire room. Furthermore, if heat losses were modelled with the duct, temperatures for case 2 would be reduced further.

These differences would have an important affect on a fire engineering assessment and any conclusions and requirements from such an assessment. For example, without the FDS calculation accounting for a mass of air within the ventilation system, oxygen availability-related phenomena may be over-predicted. These include extinction, incomplete combustion, reductions in tenability, and cooling by ambient air - all of which may be under-predicted.



(a) Case 1.



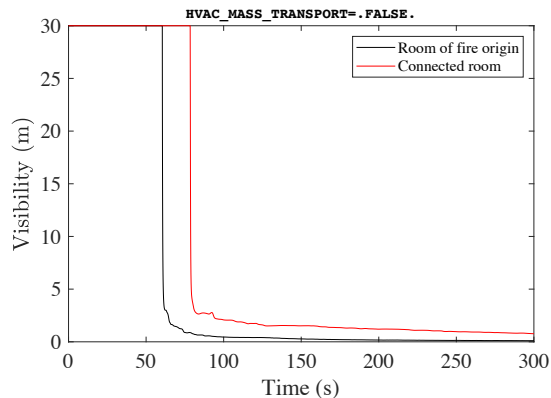
(b) Case 2.

Figure 19: Head height temperature in proximity to the exit for the two cases.

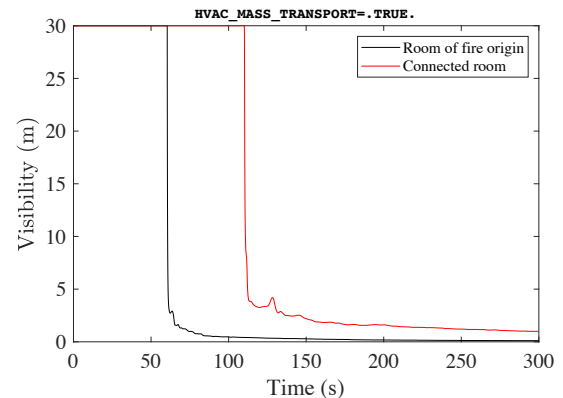
5.3.3 Head height visibility at exit

Figure 20 presents the predicted head height visibility at the exits for the two cases. Figure 20a demonstrates a very rapid drop in predicted visibility in the connected room, shortly after that in the fire room. This is because case 1 does not account for transient transport of gaseous products through the HVAC network subdomain. All mass and energy entering the ventilation system in the fire room is instantly transported into the connected room. Figure 20b illustrates that the reduction in predicted visibility in the room of fire is similar to that of case 1 but there is a difference in the predicted visibility in the connected room. The predicted visibility at head height in the connected room decreases at approximately 110s. This result is due to the ability of the case 2 calculation to account for transient transport of gas phase products through the ventilation system modelled within the HVAC network submodel. Compared to case 1 whereby all products are instantly transported to the connected room from the fire room.

Again the calculations from case 1 and case 2 would lead to a different fire engineering analysis and conclusions. For example, if relying upon the output of case 1, the analysis would under-predict the ASET within the connected room and lead to an over-specified automatic detection system.



(a) Case 1.



(b) Case 2.

Figure 20: Head height visibility in proximity to the exit for the two cases.

6 Closing remarks

It is known that deaths are caused by the spread of fire and smoke outside of the room of fire origin [30]. FDS version 5.5 introduced a computationally efficient way of modelling a ventilation system by way of the coupled HVAC network submodel. However, until version 6.5.3 and the introduction of the ability to predict the transient transport of mass, species and energy through the 1D network domain the HVAC subdomain held to mass or energy and transport time was not simulated.

The original HVAC submodel and the new addition of the transient transport of mass, species and energy (HVAC_MASS_TRANSPORT) have been described. Numerical verification of the new coupled hybrid model implementation has been presented and is shown to be satisfactory.

To illuminate the impact and usefulness of the new coupled hybrid model method, including the transient transport of gas phase quantities, a test case has been presented typical for a fire engineering analysis. The test case illustrates that the omission of transient transport through the HVAC network subdomain could have a drastic affect on the fire engineering assessment and affiliated conclusions and recommendations. The introduction of transient transport within the HVAC network submodel will enable fire engineers to better quantify their designs when analysing a total building system. Based upon comparison to full field cases, the reduction in wall time is approximately proportional to the reduction in the field domain. For example, if 50 % of the domain was modelled within the network subdomain, the wall time would be expected to be half that of a full field case. This is in agreement with other coupled hybrid models found within the tunnel modelling literature [17, 31, 32].

The new coupled hybrid method implemented with FDS version 6.5.3 onward continues to have limitations. Currently no heat loss is modelled within the HVAC network subdomain. This is expected to lead to higher predicted temperatures at HVAC-connected vents. Although the HVAC ducts have a volume and contain a mass of gas, HVAC are zero dimensional with zero volume. This functionality could be expanded to enable rooms, larger spaces, or corridors to be simply modelled within the HVAC network subdomain. There is potential for a two zone model to be introduced within the HVAC nodes for further expansion of the coupled hybrid model's capability. Combustion is not currently modelled within the network subdomain. In this manner, fuel gases which move from the field domain to the network domain only combust when re-entering the field domain.

As with all numerical models - benchmarking and validation are key stages in the safe and conscientious adoption and use of the simulation tool. To address this, a campaign of medium-scale experiments has been designed and carried out. The novel experimental rig is called Two box Will Only Behave when Operated Xerothermically (Two Box). Presentation of the experimental campaign and affiliated benchmarking exercises is lengthy and will be presented in future work. Notwithstanding, model bias factors for enclosure temperatures of 1.0, in-duct temperature of -1.4 , and in-duct velocities of $+1.4$ are put forward based upon experimental comparison. Non-fire enclosure temperatures are especially well-predicted, with numerical data falling within experimental error.

These model bias factors and benchmarking, which will be fully presented in future work, will enable a competent fire engineer to quantify model uncertainty and safely use the newly expanded model to analyse elements of the built environment.

References

- [1] G. C. Foliente, "Developments in performance-based building codes and standards," *Forest Products Journal*, vol. 50, pp. 12–21, 2000.
- [2] G. Yeoh, R. Yuen, S. Lo, and D. Chen, "On numerical comparison of enclosure fire in a multi-compartment building," *Fire Safety Journal*, vol. 38, pp. 85–94, 2 2003.
- [3] M. Ali and K. Moon, "Structural Developments in Tall Buildings: Current Trends and Future Prospects," *Architectural Science Review*, vol. 50:3, pp. 205–223, 2007.
- [4] R. Howard and B. C. Björk, "Building information modelling - Experts' views on standardisation and industry deployment," *Advanced Engineering Informatics*, vol. 22, no. 2, pp. 271–280, 2008.
- [5] H. T. Z. Kodur V. K. R., *SFPE Handbook of Fire Protection Engineering*. New York: Springer, fifth edit ed., 2016.

- [6] Department for Communities and Local Government, “Fire Statistics: Great Britain April 2012 to March 2013,” 2013.
- [7] M. Ahrens, “Home Structure Fires,” *National Fire Protection Association*, vol. Available, no. September, p. 139, 2016.
- [8] A. M. Hasofer and I. Thomas, “Analysis of fatalities and injuries in building fire statistics,” *Fire Safety Journal*, vol. 41, no. 1, pp. 2–14, 2006.
- [9] P. G. Holborn, P. F. Nolan, and J. Golt, “An analysis of fatal unintentional dwelling fires investigated by London Fire Brigade between 1996 and 2000,” *Fire Safety Journal*, vol. 38, no. 1, pp. 1–42, 2003.
- [10] J. G. Quintiere and C. A. Wade, “Compartment Fire Modeling,” in *SFPE Handbook of Fire Protection Engineering* (M. J. Hurley, D. T. Gottuk, J. R. Hall Jr., K. Harada, E. D. Kuligowski, M. Puchovsky, J. L. Torero, J. M. Watts Jr., and C. J. WIECZOREK, eds.), pp. 981–995, New York, NY: Springer New York, 2016.
- [11] T. M. Williams, “The need for new paradigms for complex projects,” *International Journal of Project Management*, vol. 17, no. 5, pp. 269–273, 1999.
- [12] A. Afzal, Z. Ansari, A. R. Faizabadi, and M. K. Ramis, “Parallelization Strategies for Computational Fluid Dynamics Software: State of the Art Review,” *Archives of Computational Methods in Engineering*, vol. 24, no. 2, pp. 337–363, 2017.
- [13] E. Galea, “On the Field Modelling Approach to the Simulation of Enclosure Fires,” *Journal of Fire Protection Engineering*, vol. 1, no. 1, pp. 11–22, 1989.
- [14] K. McGrattan, S. Hostikka, R. McDermott, J. Floyd, C. Weinschenk, and K. Overholt, “Sixth Edition Fire Dynamics Simulator Technical Reference Guide Volume 1: Mathematical Model,” tech. rep., NIST, 2017.
- [15] L. Formaggia, J. F. Gerbeau, F. Nobile, and a. Quarteroni, “Numerical treatment of defective boundary conditions for the Navier-Stokes Equations,” *SIAM Journal on Numerical Analysis*, vol. 40, no. 1, pp. 376–401, 2003.
- [16] P. J. Blanco, R. a. Feijóo, and S. a. Urquiza, “A unified variational approach for coupling 3D-1D models and its blood flow applications,” *Computer Methods in Applied Mechanics and Engineering*, vol. 196, pp. 4391–4410, 2007.
- [17] F. Colella, G. Rein, V. Verda, and R. Borchiellini, “Multiscale modeling of transient flows from fire and ventilation in long tunnels,” *Computers and Fluids*, vol. 51, no. 1, pp. 16–29, 2011.
- [18] M. Juntunen and R. Stenberg, “Nitsche’s method for general boundary conditions,” *Mathematics of Computation*, vol. 78, pp. 1353–1374, 9 2009.
- [19] M. Malinen, “Boundary Conditions in the Schur Complement Preconditioning of Dissipative Acoustic Equations,” *SIAM Journal on Scientific Computing*, vol. 29, pp. 1567–1592, 1 2007.
- [20] C. Runge, “Ueber die numerische Auflösung von Differentialgleichungen,” *Mathematische Annalen*, vol. 46, pp. 167–178, 6 1895.
- [21] J. Butcher, *Numerical Methods for Ordinary Differential Equations*. Wiley Online Library, 3rd editio ed., 2016.
- [22] S. Godunov, “A difference method for numerical calculation of discontinuous solutions of the equations of hydrodynamics,” *Matematicheskii Sbornik. Novaya Seriya*, vol. 47, no. 89, pp. 271 – 306, 1959.
- [23] American Society for Testing and Materials, “ASTM E1355-12, Standard Guide for Evaluating the Predictive Capabilities of Deterministic Fire Models,” 2012.
- [24] CIBSE, “Guide E: Fire engineering,” *The Chartered Institution of Building Services Engineers, London, UK*, 2010.
- [25] A. Handbook, “HVAC applications,” *ASHRAE Handbook, Fundamentals*, 2007.

- [26] BSRIA, “Guide to HVAC Building Services Calculations,” 2007.
- [27] B. Munson, D. Young, and T. Okiishi, *Fundamentals of fluid mechanics*. Hoboken, NJ: John Wiley & Sons, 8th ed., 2006.
- [28] CIBSE, *CIBSE Guide B0 - Applications and activities : HVAC strategies for common building types*. CIBSE, 2016.
- [29] M. Janssens and H. C. Tran, “Data Reduction of Room Tests for Zone Model Validation,” *Journal of Fire Sciences*, vol. 10, no. 6, pp. 528–555, 1992.
- [30] F. S. Zntemctisnul, “The causes of death in fire victims,” *Forensic Science International*, vol. 24, no. 2, pp. 3–7, 1984.
- [31] J. Prince and J. Peiro, “Application of a Lagrange multiplier approach for flow rate defective boundary conditions in a finite volume framework,” in *Proceedings of the 23rd UK Conference of the Association for Computational Mechanics in Engineering*, (Swansea, Wales), pp. 207–210, 2015.
- [32] D. J. Burton, A. Grandison, M. Patel, E. Galea, and J. Ewer, “Development of a Hybrid Field/Zone Fire Model,” in *Fire Safety Science-Proceedings Of The Tenth International Symposium*, pp. 1373–1386, International Association for Fire Safety Science, 2011.